Suspension Fault Diagnostics Using Vehicle Pitch and Roll Models

Xinyu Du[1], Lichao Mai[2], and Hossein Sadjadi[3]

[1,2]*General Motors Research & Development, Warren, MI, 48092, USA*
xinyu.du@gm.com
lichao.mai@gmail.com

[3]*General Motors Canadian Technical Center, Markham, Ontario, L3R 4H8, Canada*
hossein.sadjadi@gm.com

ABSTRACT

The vehicle suspension system, including springs, dampers and stabilizer bars are critical to vehicle riding and handling experience. Automatic fault detection, isolation and failure prognosis of the suspension system will greatly improve vehicle perceived quality, serviceability and customer experience. In our previous work, a static diagnostic approach using a ramp with the known slope is proposed. Even though the method can effectively isolate the suspension system faults to each vehicle corner, it requires additional setups at dealerships. In this work, a passive approach using the vehicle pitch and roll models is presented, which can accurately isolate broken springs, leaking dampers, and broken stabilizer bars. Some enabling conditions are proposed to improve the overall algorithm robustness. The proposed solution is verified using the data collected from a test vehicle.

1. INTRODUCTION

Suspension systems, including springs, dampers and stabilizer bars, are critical to the vehicle ride and handling experience. For most passenger vehicles, the main type of springs is the coil spring. The coil spring is a compression spring, which transfers the kinetic energy to the potential energy. The stabilizer bar, also called sway bar or anti-roll bar, is a type of torsion springs, which reduces the vehicle roll angle during cornering. The vehicle damper, also named shock absorber, is a hydraulic device to absorb external shock impulses. Common vehicle damper contains check valves and orifices that control the internal oil flow with an internal piston. Due to the oil viscosity and the piston resistance, when the damper is compressed, the kinetic energy is transferred to heat, which is used to reduce the shock.

The suspension components degrade overtime. Most suspension components are diagnosed by the technicians' inspection during the maintenance, which associates with labor costs and maintenance time. A real-time and accurate diagnostic solution to detect and isolate the spring, damper and stabilizer bar faults, allows early detection before failures occur. As a result, it can greatly enhance customer satisfaction and perceived quality, vehicle serviceability and availability, which in turn can reduce the warranty/repair cost and fleet maintenance cost. The common failure mode for vehicle springs is the broken spring. It may be due to corrosion, fatigue or overloading. Several diagnostic approaches for the faulty springs are proposed in (Yin & Huang, 2015), (Pravin & Sivakumar, 2019) (Muhammad & Douglas, 2005) (Zhao & Wang, 2004), (Nozaki & Inagaki, 1998), (Börner, Straky, Weispfenning, & Isermann, 2000), and (Luo, Pattipati, Qiao, & Chigusa, 2008). The main methodologies include the data driven based vehicle vibration frequency analysis and physics-model based fault characterization. The readers are referred to our previous paper for more details of spring fault diagnostics (Du, Mai, & Sadjadi, Fault Diagnostics and Prognostics for Vehicle Springs and Stablizer Bar, 2020).

The most common fault of the vehicle damper is the oil leakage, due to the accidents or the material fatigue. When it occurs, the functionality of dampers is affected, which results in a bouncier driving experience, and the driver may feel vibration of the steering wheel. There exist some papers on vehicle damper diagnostics. One common method is the vibration-based frequency analysis. A diagnostic solution, which employs the Fast Fourier Transform (FFT) and the cross-spectrum graphs, is described in (BIAŁKOWSKI & KRĘŻEL, 2017). Accelerometers are mounted on the vehicle, and the vibration response is analyzed. The vibration amplitudes of each test are calculated using the spectrum analysis. The coefficient is then calculated using the maximum amplitude of each test divided by the band power. For the faulty damper, the coefficient is significantly higher than the one generated from the healthy damper, which

indicates that it is a good fault signature to detect the damper faults. Another method by monitoring the magnitude of the system vibration frequency is introduced in (Alcantara, Brooks, Lopez , Menendez, & Mendoza, 2013). The semi-active suspension scheme is built using the magneto-rheological damper. The damper faults can be identified from the information of specific frequency ranges and a road profile amplitude compensation. As a baseline, the road profile amplitude in frequency domain can be established using acceleration data with healthy dampers. The faulty damper causes the magnitude of the suspension system resonance peaks to increase, which can also be identified from the bode diagram. In another word, the suspension system with faulty dampers shows the higher magnitude of steady state frequency response when passing the same road profile, which is used for damper faults detection. Recently, machine learning techniques are also applied in damper diagnostics. One typical approach using the Convolutional Neural Networks is shown in (Zehelein, Pottmann, & Lienkamp, 2020). The vehicle driving data, such as longitudinal acceleration and wheel speeds, and the vehicle damper health states are collected and processed after trend removal. FFT is applied for the vibration frequency analysis. Frequency features, such as peak spectrum amplitudes and corresponding frequencies, of every unique vehicle configuration with different damper effects are classified. The actual classification is performed in the fully connected layer using the averaged frequency analysis data points. The experiment results show a high accuracy for damper fault detection. Another solution proposed in (Koláček & Dostál, 2013) employs the tire force information for damper diagnostics. The test vehicle is placed on the vibration platform with the known vibration frequency. The contact forces on the tire are measured to characterize the efficiency of external shock compensation by dampers. The experiments with the faulty damper show longer tire force oscillation time and higher frequency of the tire force variation. However, this solution requires a specific test platform and technicians to perform the measurement and analysis, which may be costly for a large fleet of vehicles.

For the stabilizer bar fault diagnostics, to the best of our knowledge, there is no paper published.

In summary, there is no established method that is both fast and accurate. To bridge the gap, we proposed a static ramp test scheme (Du, Mai, & Sadjadi, Fault Diagnostics and Prognostics for Vehicle Springs and Stablizer Bar, 2020) in 2020 to quickly detect and isolate spring and stabilizer bar faults. Even though the diagnostic results are accurate (97.6% accuracy and 0% false positive rate on 82 test data sets collected from a test vehicle), this solution requires a ramp setup at each service location. In this work, we propose a passive monitoring solution to detect and isolate suspension faults on the go. The solution is based on the vehicle pitch and roll models on selected acceleration maneuvers or lane change/cornering maneuvers. For the rest of this paper, the details of the proposed solution are presented in Section 2, and the validation with real vehicle data are presented in Section 3. Section 4 concludes the paper.

2. SUSPENSION PASSIVE DIAGNOSTICS ALGORITHM

In this section, the suspension passive diagnostics algorithm is introduced, including the theoretical analysis using the pitch model and roll models, fault signature extraction, and the isolation algorithm.

The vehicle pitch model (Turco, Borodani, & Klaarenbeek , 1997) (Jin, Yin, & Chen, 2019) is used to represent the chassis dynamic behavior, when the vehicle is under an acceleration maneuver. In this scenario, the pitch angle is increasing. Shown in Figure 1, M, C_G and h are the total vehicle mass, the central gravity (CG) and the height of CG of the vehicle, respectively. F_1 and F_2 are the traction force for the rear tires and the front tires, respectively. a_x is the longitudinal acceleration. p is the pitch angle of the vehicle. K_p and C_p are the pitch stiffness constant and the pitch damping constant, respectively.

According to the Newton's second law for rotation, the dynamic equation of vehicle chassis during acceleration maneuver can be represented as follow:

$$I_y\ddot{p} + C_p\dot{p} + K_p p = Mha_x \tag{1}$$

where, p, $\dot{p}$ and $\ddot{p}$ are the pitch angle, pitch rate and pitch acceleration, respectively. I_y is the moment of inertia around the CG (lateral direction). K_p and C_p are the pitch stiffness constant and the pitch damping constant of the vehicle, respectively. As shown in the above equation, I_y, M and h are the intrinsic properties of vehicle. The value of $\dot{p}$, $\ddot{p}$ and a_x can be measured by the inertial measurement unit (IMU). The p is calculated from the integration of $\dot{p}$ in a given time period after bias removal. During the steady state, where the value of $\dot{p}$ and $\ddot{p}$ are very small, the values of $I_y\ddot{p}$ and $C_p\dot{p}$ are small and can be neglected. Then the pitch model Eq. (1) can be simplified as follows:

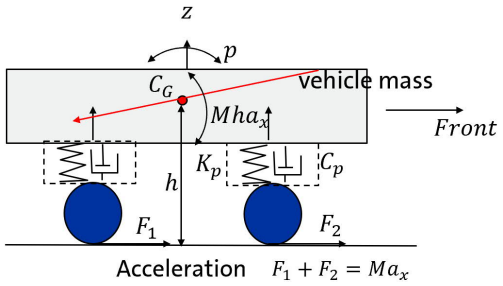

Figure 1. Simplified schematics for a vehicle during acceleration (side view)

$$K_p p = Mha_x \quad (2)$$

With Eq. (2), K_p can be estimated from the estimated p and measurement a_x. When the vehicle spring is faulty, the stiffness of the suspesion system will change. The stiffness of the spring, k, is calculated from the following equation (Probert & Hendry, 1986),

$$k = \frac{Gd^4}{8ND^3} \quad (3)$$

where, G and d are the modulous and the wire diameter of the spring steel, respectively. D is the mean coil diameter. N is the number of active coils. If the spring is broken, the length of coil will decrease, followed by the decrease of the number of active coils, N. Based on the equation, if N is decreased while the other paremeters remain the same, the value of spring stiffness k will increase, and the suspension becomes stiffer. In another word, the broken spring will increase the pitch stiffness. Therefore K_p is a good fault signature for spring faults detection.

After the K_p is calculated, the damping coefficient $C_p$can be estimated using the Eq. (1) and the polynomial curve fitting method. To perform the curve fitting, the Eq. (1) is converted to the format shown in Eq. (4), which can be further simplified as Eq. (5), where the X is the $\dot{p}$ and the Y corresponds to the terms on the left side of Eq. (3). The only unknown parameter is the C_p, which can be estimated by the polynomial curve fitting method. This part will be described in the following paragraphs.

$$Mha_x - K_p p - I_y \ddot{p} = C_p \dot{p} \quad (4)$$

$$Y = C_p X \quad (5)$$

When oil leakages of vehicle dampers occur, the defective piston rod seal leads to oil loss, which in turn reduces the damping force. If the damping force is decreased, the pitch damping constant will decrease as well.

Similarly, the vehicle roll model is used to represent the chassis dynamic behavior, when the vehicle is under the cornering or lane change maneuvers. The theoretical analysis of the vehicle roll model is shown in Figure 2.

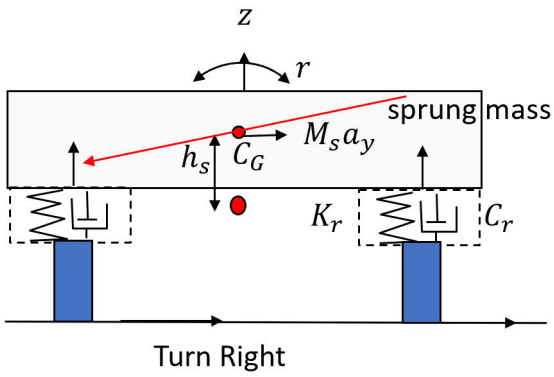

Figure 2. Simplified schematics for a vehicle during corning (rear view)

For the roll model (Turco, Borodani, & Klaarenbeek , 1997) (Jin, Yin, & Chen, 2019), M_s is the sprung mass of the vehicle, which is the vehicle mass portion supported by the suspension components and the tires. h_s is the distance of CG height above the roll axis of the vehicle. a_y is the lateral acceleration. r is the roll angle of the vehicle. K_r and C_r are the roll stiffness constant and the roll damping constant of vehicle, respectively. According to the Newton' second law for rotation, the dynamic equation during the cornering maneuver can be represented as follows:

$$(I_x + M_s h_s)^2 \ddot{r} + C_r \dot{r} + K_r r = M_s h_s a_y \quad (6)$$

where, r, $\dot{r}$ and $\ddot{r}$ are the roll angle, roll rate and roll acceleration, respectively. I_x is the moment of inertia around the CG (longitudinal direction). K_r and C_r are the roll stiffness constant and roll damping constant of vehicle, respectively. I_x, M_s and h_s are the intrinsic properties of vehicle. The value of $\dot{r}$, $\ddot{r}$ and a_y can be measured by the IMU. And r is calculated from the integration of $\dot{r}$ after bias removal. During the steady state of the lane change or cornering maneuvers, when the value of $\dot{r}$ and $\ddot{r}$ are very small, the values of $(I_x + M_s h_s)^2 \ddot{r}$ and $C_r \dot{r}$ are small and can be neglected. Then the roll model can be simplified as follows,

$$K_r r = M_s h_s a_y \quad (7)$$

Faulty stabilizer bars normally refer to the loose or the disconnection of the end link from the joint. When the stabilizer bar is disconnected, the stabilizer bar cannot provide necessary torsion force to balance the momentum, when vehicle is under the cornering maneuver. It will cause a bigger roll angle and may even lead to a vehicle rollover. In another word, the roll stiffness decreases, *i.e.* K_r is smaller. Therefore K_r is a good fault signature for stabilizer bar fault detection.

To achieve the real-time signal processing and generate the suspension diagnostics results, a diagnostic and isolation algorithm is developed, which includes two main parts, the data processing and fault diagnostics.

When the vehicle starts, the data processing is running continuously, which includes the data buffering, bias removal, maneuver detection and parameters calculation, as shown in Figure 3. The buffer is firstly reset, and the vehicle signals are continuously processed, including the a_x, a_y, $\dot{p}$, $\ddot{p}$, $\dot{r}$, $\ddot{r}$ and yaw rate ($\dot{\psi}$). The frequency of the data acquisition in this work is 100 Hz. The above signals are then automatically saved in a moving buffer that can store the latest 13 seconds of data. The pitch model and the roll model, discussed in the previous section, are then employed to analyze the data.

The data during the acceleration maneuver are recorded for the pitch model. The vehicle signals used in the pitch model are a_x and $\dot{p}$. The enabling condition to determine an acceleration maneuver is shown as follows:

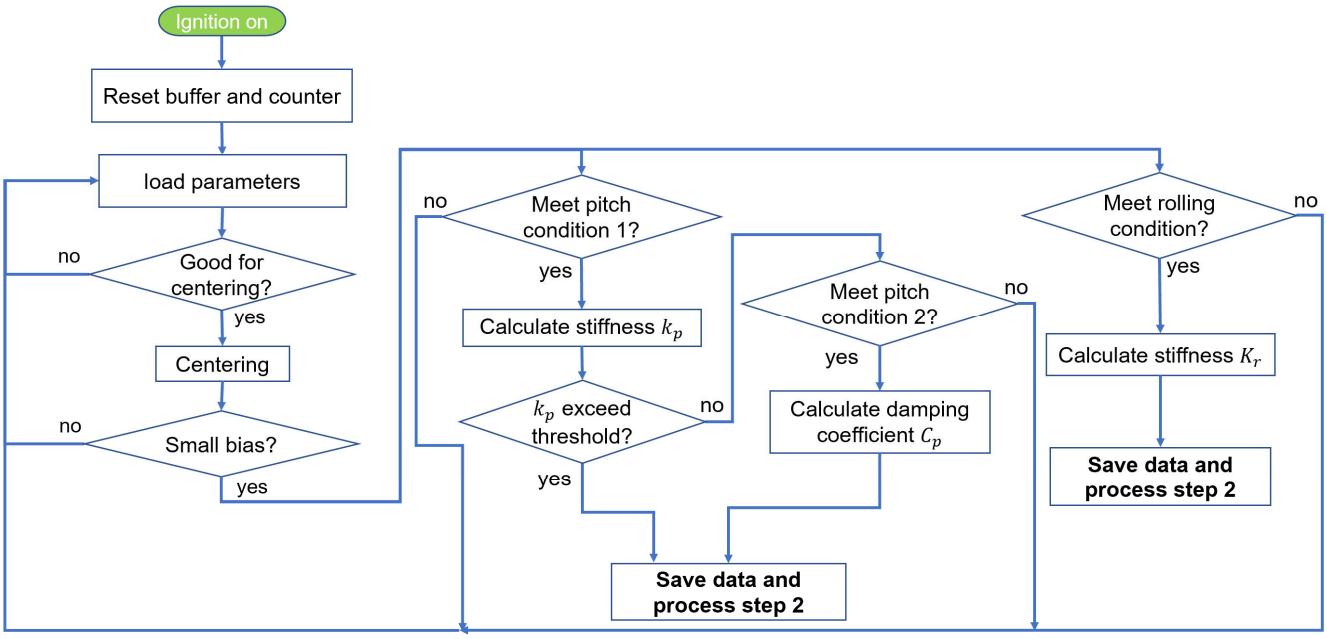

Figure 3. Flowchart of the suspension passive diagnostics algorithm (step 1: vehicle data processing)

$$a_x > T_1 \tag{8}$$

Where T_1 is a threshold to determine whether an acceleration maneuver occurs. All thresholds in the following paragraphs are presented using symbol T. Due to measurement bias, the vehicle signals should be centered each time. The signal centering (bias removal) is performed, using vehicle's steady state values before the identified acceleration maneuver. The data point in the first 2 seconds, where 2 is a calibration parameter, are processed with the following enabling condition,

$$max(|\dot{p}|) < T_2 \tag{9}$$

$$max(|a_x|) < T_3 \tag{10}$$

$$mean(|a_x|) < T_4 \tag{11}$$

If the above enabling conditions are satisfied, the mean value of each signal is considered to be the signal bias. In the steady state, the bias should be small, *i.e.*

$$|\dot{p}_{bias}| < T_5 \tag{12}$$

$$|a_{x,bias}| < T_6 \tag{13}$$

If the calculated bias is larger than the above thresholds, the calculated bias may not be accurate. Therefore, the diagnostic algorithm will not be activated. If the above criteria are satisfied, all the data in the buffer are subtracted by the corresponding bias.

After all signals are centered, the a_x and $\dot{p}$ signals from the 3rd second will be loaded to the pitch model. All centered a_x and $\dot{p}$ signals are processed using a low-pass filter.

To calculate $\ddot{p}$, the derivative of $\dot{p}$ is calculated with the time interval (dt) of 0.1 second. To calculate p, $\dot{p}$ is integrated with dt of 0.1 second, using Eq. (14).

$$\ddot{p}(t) = \frac{\dot{p}(t)-\dot{p}(t-1)}{dt} \tag{14}$$

$$p(t) = \int_0^t \dot{p} \cdot dt \tag{15}$$

For the lane change or cornering maneuvers, the enabling condition for the bias removal is defined as follows,

$$max\ (|\dot{r}|) < T_7 \tag{16}$$

$$\max\ (|a_y|) < T_8 \tag{17}$$

After the bias of $\dot{r}$ is calculated, all $\dot{r}_{bias}$ data are subtracted by the r ̇_bias for the further roll stiffness estimation.

During the acceleration maneuver, the pitch stiffness constant is firstly estimated. As stated in the previous paragraphs, the estimation is achieved during the steady state, where the values of $\dot{p}$ and $\ddot{p}$ are significantly small and can be neglected. A moving window is set to monitor the signals and determine the steady state. In this work, the size of the moving window is set to be 80, which is 0.8 seconds. In order to determine the steady state, the enabling conditions are set as below:

$$|mean(\dot{p})| < T_9 \tag{18}$$

$$|mean(\ddot{p})| < T_{10} \tag{19}$$

$$\left|\frac{max(p)-min(p)}{\bar{p}}\right| < T_{11} \tag{20}$$

$$\left|\frac{max(a_x)-min(a_x)}{mean(a_x)}\right| < T_{12} \quad (21)$$

$$|mean(a_x)| < T_{13} \quad (22)$$

If the enabling conditions above are satisfied, the *PitchIndex* is used to label the first data point. However, the steady state does not ensure to lead to the good estimation of the pitch stiffness constant. There exist some corner cases causing the inaccurate estimation of the pitch stiffness constant.

Figure 4 shows one corner case – spring hysteresis. The maximum a_x value appears at around 2 seconds, but the steady state is detected at around 4 seconds. There is a significant decrease of a_x before the steady state. If a_x decreases, it reflects the fact that the spring may change from the compression condition to the extension condition, which leads to the spring hysteresis.

In this scenario, the pitch stiffness estimation may vary a lot. The following constraint is added to avoid the pitch stiffness estimation. When the maximum value of a_x signal is in front of the *PitchIndex*, where the steady state locates, the difference between the maximum a_x value and the a_x value at the *PitchIndex* point, $a_{x,diff}$, should satisfy:

Constraint 1: $a_{x,diff} < T_{14}$ (23)

Similarly, there also exist corner cases that the pitch angle decreases before the steady state, which may also lead to the inaccurate estimation of the pitch stiffness constant. Another constraint is added to avoid such a phenomenon. If the maximum value of p is in front of the *PitchIndex*, the difference between the maximum p value and the p value at the *PitchIndex* point, p_{diff} should satisfy:

Constraint 2: $p_{diff} < T_{15}$ (24)

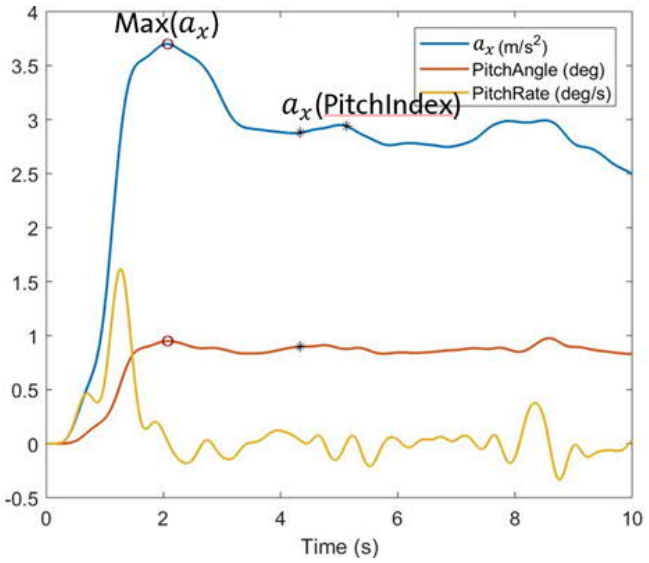

Figure 4. Acceleration maneuver for the corner case 1 (Decrease of a_x)

Based on the pitch model, a_x should be directly proportional to p during the acceleration. However, the opposite trend is found in some datasets, which is shown as Figure 5.

In Figure 5, a_{x1} and a_{x2} are the maximum a_x value and the a_x value where the *PitchIndex* locates, respectively. p_1 is the p value corresponding to the a_{x1} value, which is not necessarily referred to maximum p value. p_2 is the p value, where the *PitchIndex* locates. The $a_{x,diff1}$ is positive, while the p_{diff1} is negative, which indicates that a_x increases while p decreases. In this situation, the final estimation of the pitch stiffness constant is significantly small. To address this issue, we define Abs_sum1 as:

$$Abs\_sum1 = |a_{x,diff1}| + |p_{diff1}| \quad (25)$$

If the Abs_sum1 is small, it indicates that variations of a_x and p are small and acceptable. Otherwise, the change trend of the acceleration and the pitch angle should be the same. The overall constraint is shown as below:

Constraint 3:

$$a_{x,diff1} \times p_{diff1} > T_{16} \text{ or } Abs\_sum1 < T_{17} \quad (26)$$

Constraint 3 is based on the maximum a_x value. Similarly, another constraint should be in place based on the maximum p value. p_3 is the maximum p value before the steady state. a_{x3} is the a_x value corresponding to the p_3 value. $a_{x,diff2}$ and p_{diff2} are calculated using following equations:

$$a_{x,diff2} = a_{x3} - a_{x2} \quad (27)$$

$$p_{diff2} = p_3 - p_2 \quad (28)$$

where a_{x2} and p_2 are the corresponding values at *PitchIndex* point. We also define Abs_sum2 as follows:

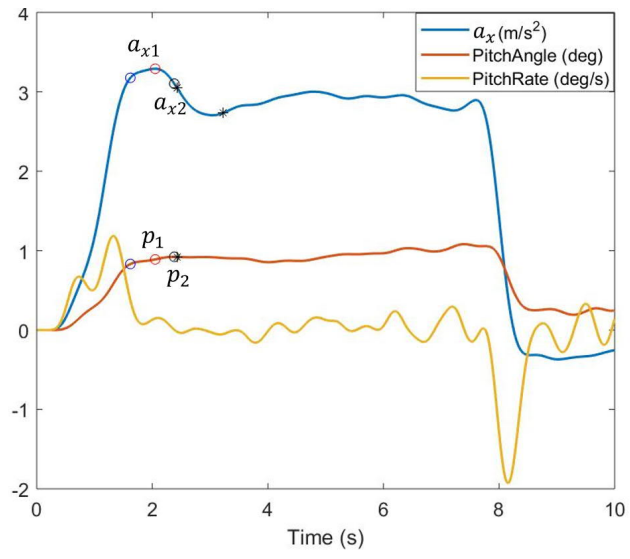

Figure 5. Acceleration maneuver for the corner case 3 (Opposite trend of a_x and p)

$$Abs\_sum2 = |a_{x,diff2}| + |p_{diff2}| \quad (29)$$

And the constraint 4 is shown as follows:

Constraint 4:

$$a_{x,diff1} \times p_{diff1} > T_{18} \text{ or } Abs\_sum2 < T_{19} \quad (30)$$

In some corner cases, a_x and p show large variation before the steady state, which causes challenges for us to determine the actual steady state. One example of such a corner case is shown in Figure 6. In the figure, index1 refers to the location where p value is 90% of the maximum p value. The corresponding a_x value is labeled as a_x (index1). In this situation, a_x changes significantly before the steady state, while p slightly changes. The variation of a_x is larger than the variation of p. Therefore, the pitch stiffness estimation will change significantly. In order to avoid such corner cases, the *ratio* 1 is defined as follows,

$$ratio\ 1 = \frac{max\,(a_x\,(index1{:}PitchIndex)) - min\,(a_x\,(index1{:}PitchIndex))}{max(p\,(index1{:}PitchIndex)) - min(p\,(index1{:}PitchIndex))} \quad (31)$$

The constraint 5 based on the ratio 1 is shown as below:

Constraint 5: $T_{20} < ratio\ 1 < T_{21}$ (32)

Please note that the thresholds of above 5 constraints are determined after the data analysis from the large number of test vehicle data. If an acceleration maneuver satisfies these constraints, the pitch model will be activated to estimate the pitch stiffness constant K_p. Otherwise, the pitch model will not be activated, and no estimation will be performed. To estimate the value of K_p, the averages of a_x and p during steady state (0.8 seconds) are calculated. Then the value of K_p is estimated using the following equation based on Eq. (2).

$$K_p = \frac{Mha_x}{p} \quad (33)$$

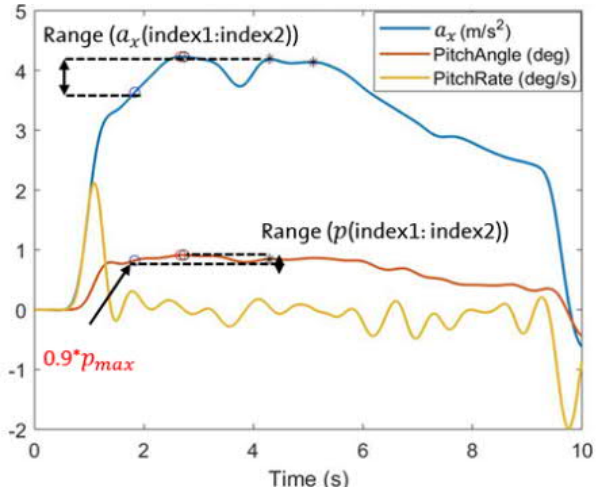

Figure 6. Acceleration maneuver for the corner case 5 (a_x large variation)

After the pitch stiffness constant K_p is estimated, the process of the pitch damping constant C_p estimation will be triggered. In this work, the estimation of C_p is performed using the linear regression. To perform the regression, the Eq. (4) and (5) are employed, where X is $\dot{p}$ and the Y is the terms on the left side of Eq. (4). The only unknown parameter is the C_p. In this work, the data selected for the curve fitting are before the steady state during an acceleration maneuver. This is also called the ramp-up state. An example curve fitting interval is shown in Figure 7. In the previous step, the steady state is determined, and the average of p_{avg} in the steady state is calculated. The start point of the ramp-up state is the location where the value of p is around 10% of p_{avg}. Similarly, the end point of the ramp-up state is the location where p is around 80% of p_{avg}. Then all signals, including p, $\dot{p}$ and $\ddot{p}$ between these two points, are selected for further analysis.

For the linear regression in this work, the length of the data is 80, which is 0.8 seconds data. After the ramp-up state is determined, another moving window is used to select the qualified data for curve fitting. The criteria are shown as following:

$$min(\dot{p}) > T_{22} \quad (34)$$

$$a_x(end) > T_{23} \quad (35)$$

$$\frac{a_x\,(end) - a_x(first)}{\text{DLD}} \times 100 > T_{24} \quad (36)$$

where DLD is data length. In a moving window for the qualified data, the value of last a_x data point in the window should be larger than 2 m/s^2, while the minimum $\dot{p}$ is larger than 0.01 deg/s. And the calculated coefficient should be larger than 1.5 m/s^2. If the above criteria are satisfied, all signals in this window are selected for curve fitting. The result is the estimated value of C_p.

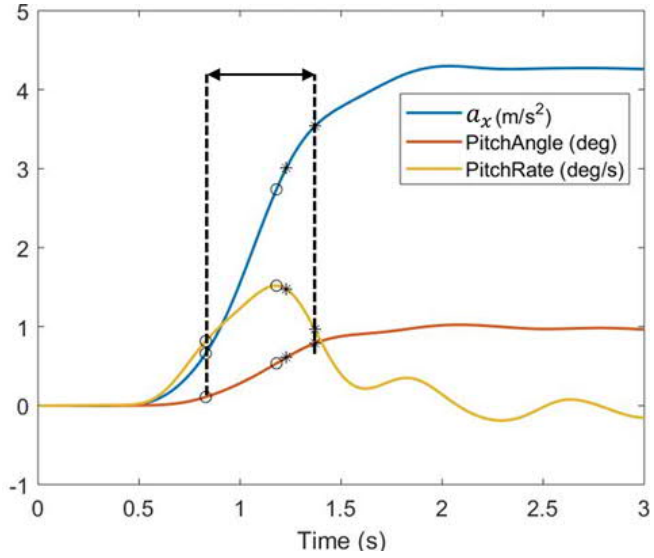

Figure 7. Polyfit interval during an acceleration maneuver

Different from the pitch model analysis, the roll model is activated, when the vehicle is running with certain speeds and under lane change or cornering maneuvers. An example of the lane change maneuver is shown in Figure 8. To detect the lane change or cornering maneuver, the yaw rate signal $\dot{\psi}$ is used as an enabling condition. If $\dot{\psi}$ at any timestamp is larger than 1 deg/s, it indicates that vehicle steering wheel is turned, and the lane change maneuver may occur. The vehicle signals within the first 2 seconds are loaded for bias removal, while the signals corresponding to the following 11 seconds are loaded for the roll model analysis.

As stated in the Eq. (7), the estimation of the roll stiffness constant is based on the simplified vehicle roll model, which can be applied during the steady state of a lane change or cornering maneuver. In order to determine the steady state, the a_y, $\dot{r}$ and $\ddot{r}$ signals are loaded and processed using the low pass filters. The r data are obtained from the previous step. In the steady state, the variations of above signals are comparatively small, and the Eq. (7) can be used to calculate the roll stiffness constant. A moving window with the size of 20 is used to look for the steady state. If, within a moving window, the selected vehicle data are all satisfied with the following criteria, this interval is considered as the steady state.

$$|mean(\dot{r})| < T_{25} \tag{37}$$

$$|mean(r)| < T_{26} \tag{38}$$

$$\left|\frac{max(r)-min(r)}{mean(r)}\right| < T_{27} \tag{39}$$

$$\left|\frac{max(a_y)-min(a_y)}{mean(a_y)}\right| < T_{28} \tag{40}$$

$$|mean(a_y)| > T_{29} \tag{41}$$

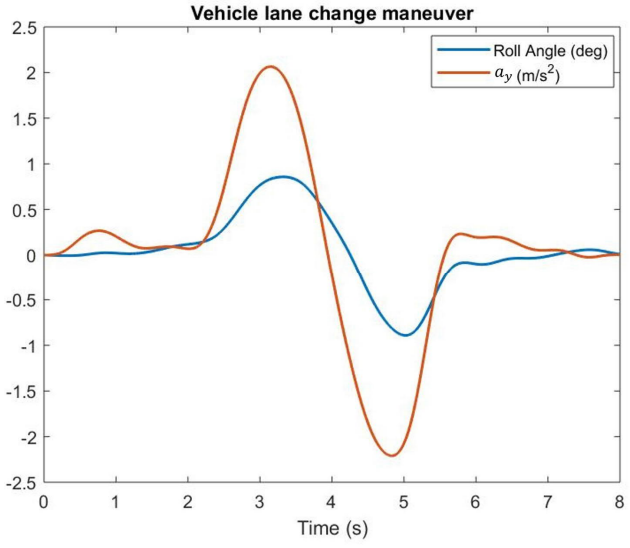

Figure 8. The example of vehicle lane change maneuver

After the steady state is determined, the a_y and r signals in this interval can be used to calculate the roll stiffness constant K_r, using the following equation.

$$K_r = \frac{M_s h_s a_y}{r} \tag{42}$$

The calculated K_r will be then saved in the buffer. The estimated the health indicators K_p, C_p and K_r, are then saved in the buffer. Each calculated parameter is considered as one available result. In another word, there are 3 buffers to separately save the K_p, C_p and K_r results. The diagnostics algorithm continuously monitors the results in each buffer. If any buffer has at least 6 available results, the diagnostics algorithm will be activated, and the corresponding parameters will be loaded.

Please note that only the buffer with at least 6 available results is processed. If a buffer with less than 6 available results, the data in that buffer will not be processed with the diagnostics algorithm. After the results are loaded, the average of these results is calculated, which are labeled as $K_{p,a}$, $C_{p,a}$ and $K_{r,a}$, respectively.

If the $K_{p,a}$ is smaller than the threshold T_{Kp}, it indicates that the vehicle spring is healthy. Otherwise, it indicates that the spring is faulty, and the diagnostics result will be reported. If the $K_{r,a}$ is available, which is generated from the previous 6 K_r results, $K_{r,a}$ is compared with the threshold T_{Kr}. If $K_{r,a}$ is larger than T_{Kr}, it indicates that the stabilizer bar is healthy.

If $C_{p,a}$ is larger than the threshold T_{Cp}, it indicates that the vehicle damper is healthy. Otherwise, the vehicle damper is considered as faulty and the diagnostics results will be reported. All these thresholds should be calibrated for different suspensions systems.

3. ALGORITHM VALIDATION

To verify the proposed diagnostics algorithm, the test data during 1,721 acceleration or lane change maneuvers are collected from a test vehicle with springs, dampers and stabilizer bars in different health conditions. Among these test data, 210 are under the condition of one faulty spring, 248 are under the condition of the disconnected stabilizer bar, 222 are under the condition of one leaking damper, and 558 are under the healthy vehicle condition. In this paper, only the single point failure is considered. Here the leaking damper means 50% or 75% loss of damper oil, and the faulty spring means the bottom coil of the spring is removed (front springs), or two/three coils of springs are clamped together (rear springs). For each acceleration maneuver, the longitudinal acceleration is between 0.2g and 0.4g. For each lane change maneuver, the lateral acceleration is between 0.1g and 0.3g.

With regard to spring diagnostics, 411 test data with healthy components, 80 test data from disconnected stabilizer bar and 222 test data from leaking damper are labeled as healthy

spring data. 210 test data from faulty springs are labeled as faulty spring data. Our diagnostic results for the spring diagnostics are shown in Figure 9. In these three figures, the "ground truth" is the actual test vehicle condition, and the "prediction" is the diagnostic result from the algorithm.

With regard to stabilizer bar diagnostics, 558 test data with healthy components, 214 test data from faulty springs and 226 test data from leaking damper are labeled as healthy stabilizer bar data. 82 test data from disconnected stabilizer bar are labeled as faulty stabilizer bar data. Our diagnostic results for the stabilizer bar are shown in Figure 10.

With regard to damper diagnostics, 411 test data with healthy components, 210 test data from faulty springs and 248 data from disconnected stabilizer are labeled as healthy damper data. 222 test data from leaking damper bar are labeled as faulty damper data. Our diagnostic results are shown in Figure 11.

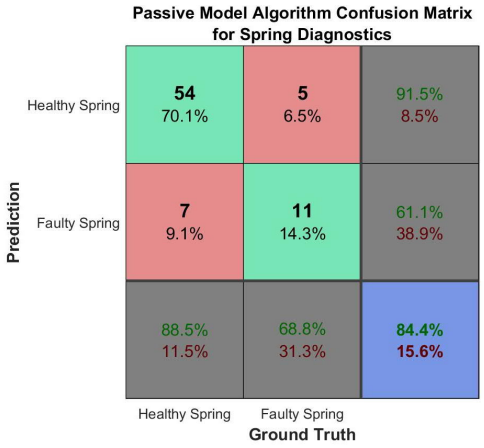

Figure 9. Algorithm confusion matrix for the spring diagnostics

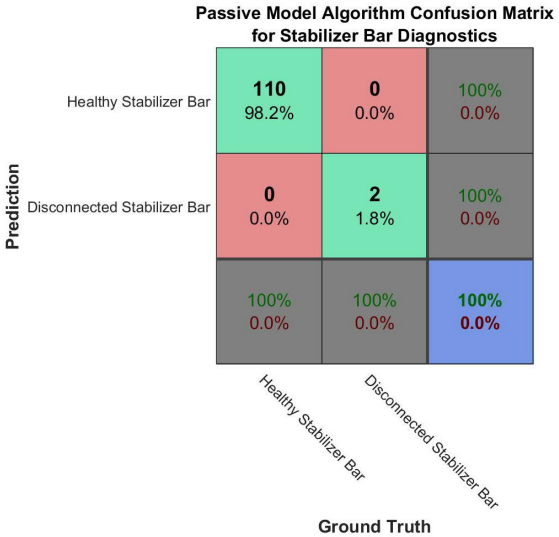

Figure 10. Algorithm confusion matrix for the stabilizer bar diagnostics

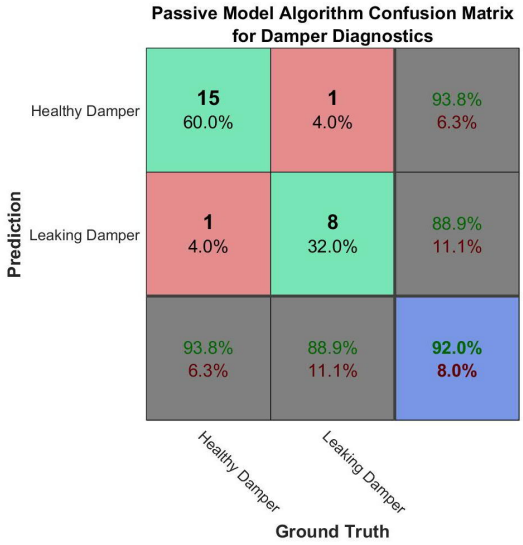

Figure 11. Algorithm confusion matrix for the damper diagnostics

Due to the enabling conditions and constraints for the maneuvers, some test results are not qualified, and no diagnostic result is generated. For example, 83 test data are filtered out due to the large calculated bias before the acceleration maneuver, which fails to satisfy the enabling condition. All qualified results are processed using the moving average. Please note that each diagnostic decision is based on 6 qualified results. The algorithm generates 77 decisions for spring diagnostics, 25 decisions for damper diagnostics and 112 decisions for stabilizer bar diagnostics.

The overall accuracy of the algorithm is calculated as the total number of correct diagnostic results (the same as the ground truth) divided by the total number of vehicle tests. The accuracy is 84.4% for spring diagnostics, 92% for damper diagnostics and 100% for stabilizer bar diagnostics. The false positive rate (FPR) reflects the percentage of actual healthy cases that are incorrectly identified as faulty cases. The FPR is 30.43% for spring diagnostics, 10% for damper diagnostics and 0% for stabilizer bar diagnostics. The false negative rate (FNR) indicates the percentage of actual faulty cases that are incorrectly diagnosed as healthy cases. The FNR is 7.58% for spring diagnostics, 5.88% for damper diagnostics and 0% for stabilizer bar diagnostics.

To further explore the noise factors that may affect the performance of the proposed algorithm, some robustness tests are conducted. Main noise factors include acceleration on the ramp, low tire pressure, driving on the rough road and different vehicle weights.

In the previous tests, the acceleration maneuvers normally occur on the flat ground. However, if the acceleration maneuver occurs on uphill or downhill, the vehicle pitch angle changes according, which may affect the estimation of K_p and C_p. To validate algorithm robustness, 15 acceleration

tests are performed on a 7.2% grade ramp. No false positive alert is found.

Tire pressure is another main factor that may affect the algorithm performance. Normally, the tire pressure of test vehicle is 35 psi. Low tire pressure may change the vehicle corner height and further affect the pitch angle. The first tests are performed using the healthy vehicle with the FL low tire pressure (22 psi). No false positive alert is found. The second tests are performed using the healthy vehicle with four ties low pressure (22 psi). No false positive alert is found. In summary, the low tire pressures (22 psi) do not affect the accuracy of the algorithm.

A rough road with uneven road surfaces is selected to perform the road tests, including acceleration and lane change maneuvers. No false positive alert is found. The last robustness test is to increase the vehicle weight. The normal weight of the test vehicle with a driver and a passenger is 1600 kg. In the robustness test, 320 lbs. (145 kg) sandbags are loaded to the rear seats of the vehicle, to simulate the situation of two more passengers on the vehicle. The total vehicle weight is now 1745 kg. Several road tests are performed, and no false positive alert is found.

4. CONCLUSION

A real-time and passive approach is developed in this work to detect and isolate broken springs, leaking dampers and disconnected stabilizer bars. We demonstrate that the spring faults can be characterized by the fault signature, vehicle pitch stiffness constant, which is estimated from the longitudinal acceleration and the pitch rate during the steady state of longitudinal acceleration. The damper faults can be characterized by the fault signature, vehicle damping constant, which is estimated from the longitudinal acceleration and the pitch rate during the dynamic state of longitudinal acceleration. The stabilizer bar faults can be characterized by the fault signature, vehicle roll stiffness constant, which is estimated from the lateral acceleration and the roll rate in the steady state of lateral acceleration. A set of unique enabling conditions is employed to improve algorithm robustness, which includes the stationary driving maneuver detection for sensor bias removal, stationary acceleration detection for stiffness calculation, dynamic acceleration detection for damping constant calculation and hysteresis scenario detection to improve robustness. A novel fault isolation process is proposed to generate accurate results. Compared with state-of-art approaches, our method is fast and accurate and is capable of isolating three different suspension failures.

Based on 214 diagnostics results generated from 1,721 test cases collected from a test vehicle, the accuracy of the suspension passive diagnostics algorithm is 84.4% for spring diagnostics, 92% for damper diagnostics and 100% for stabilizer bar diagnostics. The false positive rate is 30.43% for spring diagnostics, 10% for damper diagnostics and 0% for stabilizer bar diagnostics. In the future, more robustness tests will be performed. We will further study the algorithm performance variations among different vehicles and different programs. The final algorithm will be developed and integrated with other chassis diagnostics, *e.g*. the rotor diagnostics (Du, Mai, Kazemi, & Sadjadi, 2020) and the wheel bearing diagnostics (Feng, Du, & Salman, 2019).

REFERENCES

Zehelein, T., Pottmann, T. H., & Lienkamp, M. (2020). Diagnosing Automotive Damper Defects Using Convolutional Neural Networks and Electronic Stability Control Sensor Signals. *Journal of Sensor and Actuator Networks, 9*, 8.

Alcantara, D. H., Brooks, L. A., Lopez , C. V., Menendez, R. M., & Mendoza, R. R. (2013). Fault detection for automotive semi-active dampers. *2013 Conference on Control and Fault-Tolerant Systems (SysTol)*, (pp. 625-630). Nice.

BIAŁKOWSKI, P., & KRĘŻEL, B. (2017). Diagnostic of shock absorbers during road test with the use of vibration FFT and cross-spectrum analysis. *Diagnostyka, 18*, 79-86.

Börner, M., Straky, H., Weispfenning, T., & Isermann, R. (2000). Model Based Fault Detection of Vehicle Suspension and Hydraulic Brake Systems. *IFAC Proceedings Volumes, 33*(26), 1073-1078.

Du, X., Mai, L., & Sadjadi, H. (2020). Fault Diagnostics and Prognostics for Vehicle Springs and Stablizer Bar. *Annual Conference of the PHM Society, 12.*

Du, X., Mai, L., Kazemi, H., & Sadjadi, H. (2020). Fault Detection and Isolation for Brake Rotor Thickness Variation. *Annual Conference of the PHM Society, 12.*

Feng, J., Du, X., & Salman, M. (2019). Wheel Bearing Fault Isolation and Prognosis Using Acoustic Based Approach. *Annual Conference of the PHM Society, 11*.

Jin, X., Yin, G., & Chen, N. (2019). Advanced Estimation Techniques for Vehicle System Dynamic State: A Survey. *Sensors, 19*(19), 4289.

Koláček, S., & Dostál, P. (2013). Evaluation of dampers using a resonance adhesion tester. *Acta Universitatis Agriculturae et Silviculturae Mendelianae Brunensis, 61*(6), 1749-1753.

Luo, J., Pattipati, K. R., Qiao, L., & Chigusa, S. (2008). Model-Based Prognostic Techniques Applied to a Suspension System. *IEEE Transactions on Systems, Man, and Cybernetics - Part A: Systems and Humans, 38*, 1156-1168.

Muhammad, A., & Douglas, H. E. (2005). Active and Event-Driven Passive Mechanical Fault Identifcation in Ground Vehicle Suspension Systems. *ASME 2005*

International Mechanical Engineering Congress and Exposition, 74. Orlando.

Nozaki, H., & Inagaki, Y. (1998). Measuring and diagnosis technology on shock absorber damping force and coil spring constant, when a shock absorber and coil spring being equipped with a car. *Jidosha Gijutsukai Gakujutsu Koenkai Maezurishu*, 117-120.

Pravin, K., & Sivakumar, B. (2019). Online Model for Suspension Faults Diagnostics Using IoT and Analytics. *International Conference on Advanced Computing, Networking and Informatics, 870.* Indore, India.

Probert, C., & Hendry, J. (1986). Carbon fiber coil springs. *Materials and Design, 6*, 330-337.

Turco, P., Borodani, P., & Klaarenbeek , F. W. (1997). Algorithms for a Vehicle Dynamics Monitoring System, Based on Model Reference Structure. *Meccanica*, 449-457.

Yin, S., & Huang, Z. (2015). Performance Monitoring for Vehicle Suspension System via Fuzzy Positivistic C-Means Clustering Based on Accelerometer Measurements. *IEEE/ASME Transactions on Mechatronics, 20*, 2613-2620.

Zhao, W., & Wang, L. (2004). Nonlinear fault diagnosis on vehicle system in the spring broken down. *IEEE, 2*, 1650-1653.

BIOGRAPHIES

Xinyu Du received B.Sc. and M.Sc. degrees in automation from Tsinghua University, Beijing, China, in 2001 and 2004, respectively, and a Ph.D. in electrical engineering from Wayne State University, MI, USA, in 2012. He has been working at General Motors Global R&D Center, Warren, MI, since 2010, and currently holds the staff researcher position in the vehicle systems research lab. His research interests include fuzzy hybrid system, vehicle health management, deep learning and data analytics. He has published more than 40 peer review papers and holds 56 patents or patent applications. He has been serving as an associate editor for Journal of Intelligent and Fuzzy Systems from 2012 and IEEE Access from 2018. He received the Boss Kettering Award from General Motors for his contribution in integrated starting system prognosis in 2015.

Lichao Mai received dual B.S. degree in automotive engineering from Wuhan University of Technology, Wuhan, China, in 2016, and in mechanical engineering from the University of Missouri, MO, USA, in 2016, respectively. He received a M.S. degree in mechanical engineering from the University of Texas at Austin, TX, USA, in 2018. He has been working at General Motors Global R&D Center, Warren, MI, since 2018. His research interests include vehicle health management, autonomous driving and data analytics.

Hossein Sadjadi received his Ph.D. degree in electrical engineering from Queen's University, Canada, and M.Sc. degree in mechatronics and B.Sc. degree in electrical engineering from the American University of Sharjah, UAE. He has been working at General Motors, Canadian Technical Center, Markham, ON, since 2017, and is currently the Engineering Lead and Feature Owner for Vehicle Health Management. He also had served as a post-doctoral medical robotic researcher at Queen's university, senior automation engineer for industrial Siemens SCADA/DCS solutions, and senior mechatronics specialist at AUS mechatronics center. His research interests include autonomous systems and medical robotics. He has published numerous patents and articles in these areas, featured at IEEE transactions journals, and received several awards.